Advanced 3D Monte Carlo Algorithms for Biophotonic and Medical Applications

Lewis McMillan

University of
St Andrews

This thesis is submitted in partial fulfilment for the degree of
PhD
at the
University of St Andrews

March 2019

Declaration

I, Lewis McMillan, hereby certify that this thesis, which is approximately ***** words in length, has been written by me, that it is the record of work carried out by me, or principally by myself in collaboration with others as acknowledged, and that it has not been submitted in any previous application for a higher degree.

I was admitted as a research student in September 2015 and as a candidate for the degree of PhD in September 2015; the higher study for which this is a record was carried out in the University of St Andrews between 2015 and 2019.

Date . . . .   Signature of candidate . . . .

I hereby certify that the candidate has fulfilled the conditions of the Resolution and Regulations appropriate for the degree of PhD in the University of St Andrews and that the candidate is qualified to submit this thesis in application for that degree.

Date . . . .   Signature of supervisor . . . .

Date . . . .   Signature of supervisor . . . .

Abstract

Lorem ipsum dolor sit amet, consectetuer adipiscing elit. Ut purus elit, vestibulum ut, placerat ac, adipiscing vitae, felis. Curabitur dictum gravida mauris. Nam arcu libero, nonummy eget, consectetuer id, vulputate a, magna. Donec vehicula augue eu neque. Pellentesque habitant morbi tristique senectus et netus et malesuada fames ac turpis egestas. Mauris ut leo. Cras viverra metus rhoncus sem. Nulla et lectus vestibulum urna fringilla ultrices. Phasellus eu tellus sit amet tortor gravida placerat. Integer sapien est, iaculis in, pretium quis, viverra ac, nunc. Praesent eget sem vel leo ultrices bibendum. Aenean faucibus. Morbi dolor nulla, malesuada eu, pulvinar at, mollis ac, nulla. Curabitur auctor semper nulla. Donec varius orci eget risus. Duis nibh mi, congue eu, accumsan eleifend, sagittis quis, diam. Duis eget orci sit amet orci dignissim rutrum.

Nam dui ligula, fringilla a, euismod sodales, sollicitudin vel, wisi. Morbi auctor lorem non justo. Nam lacus libero, pretium at, lobortis vitae, ultricies et, tellus. Donec aliquet, tortor sed accumsan bibendum, erat ligula aliquet magna, vitae ornare odio metus a mi. Morbi ac orci et nisl hendrerit mollis. Suspendisse ut massa. Cras nec ante. Pellentesque a nulla. Cum sociis natoque penatibus et magnis dis parturient montes, nascetur ridiculus mus. Aliquam tincidunt urna. Nulla ullamcorper vestibulum turpis. Pellentesque cursus luctus mauris.

Acknowledgements

Lorem ipsum dolor sit amet, consectetuer adipiscing elit. Ut purus elit, vestibulum ut, placerat ac, adipiscing vitae, felis. Curabitur dictum gravida mauris. Nam arcu libero, nonummy eget, consectetuer id, vulputate a, magna. Donec vehicula augue eu neque. Pellentesque habitant morbi tristique senectus et netus et malesuada fames ac turpis egestas. Mauris ut leo. Cras viverra metus rhoncus sem. Nulla et lectus vestibulum urna fringilla ultrices. Phasellus eu tellus sit amet tortor gravida placerat. Integer sapien est, iaculis in, pretium quis, viverra ac, nunc. Praesent eget sem vel leo ultrices bibendum. Aenean faucibus. Morbi dolor nulla, malesuada eu, pulvinar at, mollis ac, nulla. Curabitur auctor semper nulla. Donec varius orci eget risus. Duis nibh mi, congue eu, accumsan eleifend, sagittis quis, diam. Duis eget orci sit amet orci dignissim rutrum.

Nam dui ligula, fringilla a, euismod sodales, sollicitudin vel, wisi. Morbi auctor lorem non justo. Nam lacus libero, pretium at, lobortis vitae, ultricies et, tellus. Donec aliquet, tortor sed accumsan bibendum, erat ligula aliquet magna, vitae ornare odio metus a mi. Morbi ac orci et nisl hendrerit mollis. Suspendisse ut massa. Cras nec ante. Pellentesque a nulla. Cum sociis natoque penatibus et magnis dis parturient montes, nascetur ridiculus mus. Aliquam tincidunt urna. Nulla ullamcorper vestibulum turpis. Pellentesque cursus luctus mauris.

Contents

List of Figures

x

Chapter 1

3D Phase Tracking Monte Carlo Algorithm

1.1 Introduction

Bessel beams have been the subject of intense research since their discovery in 1987 [1,2]. Durnin noticed that the blah blah.

This chapter examines how Bessel beams compare to other beam in a scattering medium. We investigate if the Bessel beams self-healing property has any effect in a turbid medium. We examine Bessel beams and the other beams by creating a novel Monte Carlo radiation transfer (MCRT) algorithm that allows the tracking of a photon as it propagates through a medium. The main focus of this chapter, is validation of our new novel technique, followed by using the new algorithm (φMC) to compare Gaussian and Bessel beams, to see which one preforms better in a turbid medium. This chapter also extends out novel algorithm to other complex, diffraction less beams

1.2 Theory

The MCRT algorithm as described in **??**, must be adjusted so that wave phenomena such as interference and diffraction can be modelled. Modelling these wave behaviours allows us to model complex beams, where these phenomena are required to form the beam, e.g Bessel beams. As MCRT is a ballistic simulation of photon packets, meaning that the MCRT simulation presented thus far in this thesis only modelled the ballistic behaviour of photons. However for the work presented in this chapter, wave like behaviour is crucial to modelling the various experiments and phenomena.

To convert a ballistic simulation of photon packets into a ballistic/wave-like simulation, the complex phase of each photon packet is tracked. This is achieved, by simply tracking the complex phase of the photon as it propagates through a medium. Equation (1.1) shows how the phase is calculated.

$$\varphi = cos\left(\frac{2\pi l}{\lambda}\right) + i \ sin\left(\frac{2\pi l}{\lambda}\right) \tag{1.1}$$

Where φ [$-$] is the phase of a photon packet, l [m] is the distance the photons has travelled, λ [m] is the wavelength of the photon, and i is the solution to $x^2 = -1$. Now we can calculate

the phase of a photon at a position P_o, if we know the distance it has travelled, and its original phase, Fig. 1.1.
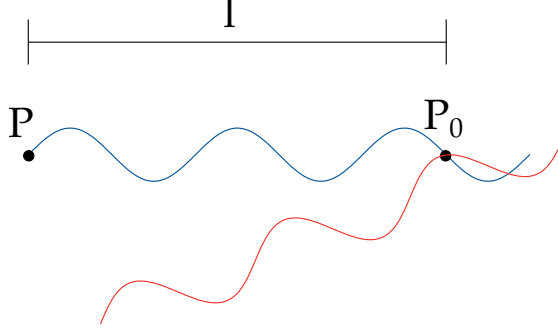

Figure 1.1: *Example of phase calculation when a photon has travelled a distance l. Figure also show an example of interference between two photons via addition of the complex amplitudes at the point P_0.*

To be able model the wave-like behaviour of photons, we let the photons packets interfere with one another in a volume or area element. We do not model the interference at a point in space where photons packets cross one another as due to the ballistic nature of the MCRT simulation, this does not occur with enough frequency in order to give a good signal to noise ratio. Thus, interference takes place in a volume, dV, or area element, dA, instead. To calculate the interference from the phase, the phase is summed in each volume or area element and the absolute value taken, and then squared. Equation (1.2) shows the equation for interference for a volume element dV. A similar relation for calculating the interference on an area element dA also exists.

$$I(\xi) = \left| \sum_{\xi} cos\left(\frac{2\pi l}{\lambda}\right) + i \sum_{\xi} sin\left(\frac{2\pi l}{\lambda}\right) \right|^2, \quad \xi = (x, y, z) \tag{1.2}$$

Where:
  l is the total distance travelled by a photon $[m]$;
  λ is the wavelength of the photon $[m]$;
  I is the intensity at the ξth cell $[Wm^{-2}]$;
  and ξ is the xth, y^{th}, z^{th} cell, volume dV.

As the MCRT simulation is now a quasi ballistic/wave simulation of photon behaviour, comparisons between the simulations and, theoretical and experimental data to prove this model is accurate. However before validation of the model takes place, one further principle needs to be introduced that is required for our model to work.

1.2.1 Huygens-Fresnel Principle

The Huygens-Fresnel principle is a method that is used to help model the propagation of waves in the far field limit and the near field limit.

The Huygens principle states [3–5]:

"Every point on a propagating wavefront serves as the source of spherical secondary wavelets, such as the source at some time later is the envelope of these wavelets."

The principle is illustrated in Fig. 1.2. Christiaan Huygens postulated this principle in 1678. The principle allowed Huygens to derive laws of refraction and reflection, but it failed to describe diffraction effects. This led to Augustin-Jean Fresnel in 1818, combining the Huygens principle with his own theory of interference [5, 6]. This principle, the Huygens-Fresnel principle, gave an accurate description of the propagation of light and diffraction effects. This was achieved by allowing the secondary wavelets to self interfere with one another, giving rise to an accurate description of the physical phenomena. Later, Gustav Kirchhoff gave a rigours mathematical description of the Huygens-Fresnel principle, which is the basis of diffraction theory [7, 8].

The Huygens-Fresnel principle allows the modelling of diffraction in both the near and far field. As the principle states that every point on the wavefront is a source of secondary spherical waves, this implies that there are "backward" waves. These "backward" waves are unphysical, and there is no evidence of their existence. Thus Fresnel introduced and inclination factor to eliminate these "backward" waves. This inclination factor was later put on rigorous mathematical standing by Kirchoff, as it naturally fell out of his theory. [7, 8]

Our algorithm uses the Huygens-Fresnel principle to simulate diffraction effects, that would otherwise be absent from the simulation. The principle allows the algorithm to calculate the complex amplitude at a point, and thus the intensity at that point. The Huygens-Fresnel principle is implemented by sampling the light source on the surface of any lens or in a slit. In practise this means when for example, a plane wave is incident on a slit width a, and length b, the slit area is uniformly sampled for the initial position of the photon packets. The packets are then given a random direction, sampled towards the detector thus avoiding the non-existent "backward" waves. For the case of modelling propahation through a lens, the usual geometric optics approach is taken to propagate the packets through the lens. When the packet lies on the surface of the lens, the Huygens-Fresnel principle is invoked, and the packet is given a random direction (in the direction of the medium) and propagated as usual.

This is the principle that underpins the algorithm that allows various complex beams, and wave phenomena to be simulated within a ballistic method. The following sections validate the method against the theory and experimental data for various complex beam propagation.
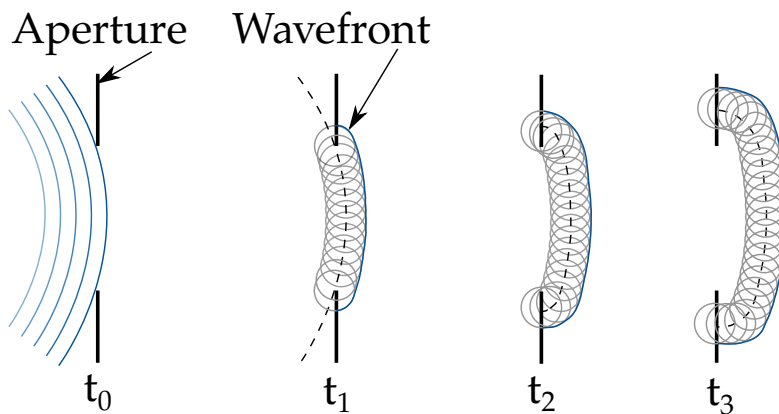

Figure 1.2: *Illustration of the Huygens-Fresnel principle. At t_0 a wave is incident on an aperture. Times t_1, t_2, and t_3 show the evolution of the wavefront using the Huygens-Fresnel principle.*

1.2.2 Validation of Phase Tracking Algorithm

Double Slit Experiment

The first test of our phase tracking algorithm, is to compare our simulation to a double slit experiment. The double slit experiment, is a simple experiment where monochromatic plane wave of light is incidence on two slits distance apart a, and width b, and the interference pattern is observed on a screen a distance d away from the slits.

This experiment, first carried out by Thomas Young and thus sometimes called Young's slits experiment, is usually carried out with the detector screen in the far field. The so called Fraunhofer regime. The intensity pattern on the detector screen is as inEq. (1.3):

$$I(\theta) \propto cos^2\left(\frac{\pi d\ sin\theta}{\lambda}\right) sinc^2\left(\frac{\pi b\ sin\theta}{\lambda}\right) \tag{1.3}$$

Where the *sinc* function is defined as $\frac{sin(x)}{x}$, for $x \neq 0$, d is the slit separation and θ is the angular spacing of the fringes.

The simulation was carried out for a wavelength of , a slit width of, and a slit separation of . Using the Huygens-Fresnel principle, each slit is a source of Huygens wavelets. The initial position of the photon packets is sampled uniformly from the slit area, after randomly choosing one of the slits. A random direction is then chosen to ensure that the packets will hit the detector screen. The simulation was run with photon packets, which took to run on an 8 core Intel Xeon machine. This gave an accurate match to the theoretical expression, as seen in Fig. 1.3.

Figure 1.3: *Comparison of theory and simulation for the double slit experiment. λ is xnm, b is, and d*

Diffraction by a Square Slit

φMC is also validated by simulating diffraction from a square aperture in the far and near field, the so call Fresnel and Fraunhofer regimes. Fresnel diffraction occurs in the near field when the *Fresnel number*, Eq. (1.4), is greater than 1.0. Fraunhofer diffraction occurs when the *Fresnel number* is less than 1.0.

$$F = l\sqrt{\frac{2}{\lambda r_0}} \tag{1.4}$$

Equation (1.4) is the Fresnel number, a measure of whether diffraction is in the Fresnel regime or the Fraunhofer regime. l is the slit width, λ is the wavelength of the incident radiation, and r_0 is the distance from the aperture to the detector screen, as shown in Fig. 1.4.

In order to compare φMC to the theory, the theory must first be examined. Consider the setup as shown in Fig. 1.4, in order to calculate the intensity at a point P, the contribution by an area element dS at the point a, to the optical disturbance at a point P is considered. Accounting for the the unobstructed optical disturbance from S as well, yields:

$$U(P) = \frac{1}{i\lambda} \iint_{\Sigma} \frac{Ae^{i(k\rho-\omega t)}}{\rho} \frac{e^{ikr}}{r} cos(\theta)\ dS \tag{1.5}$$

In the case where ρ_0 and r_0 are large compared to the size of the aperture, then $cos(\theta) = 1$ and $\frac{1}{\rho r} = \frac{1}{\rho_0 r_0}$. The lengths of r_0 and ρ_0 are:
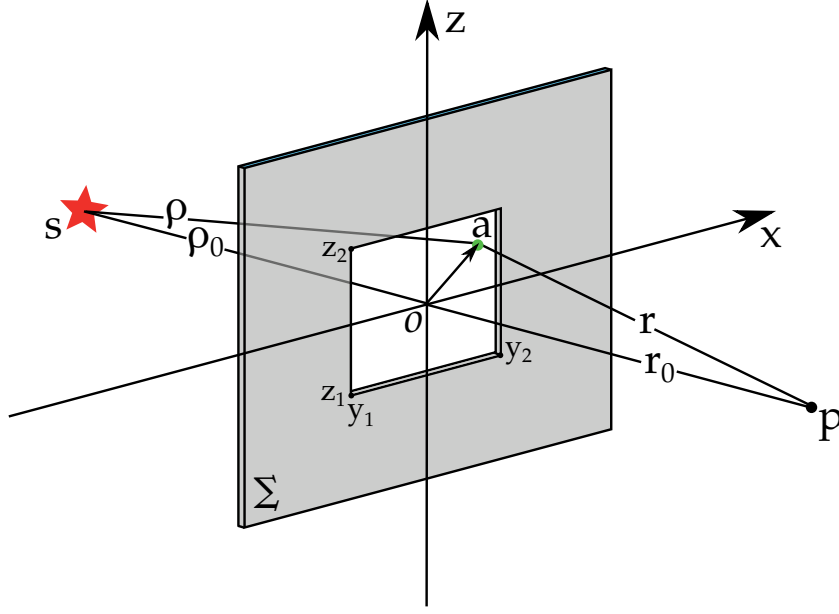
Figure 1.4: *Fresnel diffraction at a square aperture.*

$$r = \sqrt{r_0^2 + y^2 + z^2} \tag{1.6}$$

$$\rho = \sqrt{\rho_0^2 + y^2 + z^2} \tag{1.7}$$

Using the binomial theorem to expand Eqs. (1.6) and (1.7) yields:

$$\rho + r \approx \rho_0 + r_0 + (y^2 + z^2)\frac{\rho_0 r_0}{2\rho_0 r_0} \tag{1.8}$$

Substituting Eq. (1.8) into Eq. (1.5) with $k = 2\pi/\lambda$

$$U(P) = \frac{A e^{-i[k(\rho_0 + r_0)\omega t]}}{i\lambda\rho_0 r_0} \iint\limits_{\Sigma} e^{i2\pi y^2 \frac{(\rho_0 + r_0)}{2\lambda\rho_0 r_0} + i2\pi z^2 e^{\frac{i\pi u^2}{2}} \frac{(\rho_0 + r_0)}{2\lambda\rho_0 r_0}} \; dS \tag{1.9}$$

Introducing the dimensionless variables u and v

$$u = y\sqrt{\frac{2(\rho_0 + r_0)}{\lambda\rho_0 r_0}} \tag{1.10}$$

$$v = z\sqrt{\frac{2(\rho_0 + r_0)}{\lambda\rho_0 r_0}} \tag{1.11}$$

and substituting them into Eq. (1.9).

$$U(P) = \frac{\tilde{E}_u}{2} \int_{u_1}^{u_2} e^{\frac{i\pi u^2}{2}} \; du \int_{v_1}^{v_2} e^{\frac{i\pi v^2}{2}} \; dv \tag{1.12}$$

5

Equation (1.12) describes the optical disturbance at the point P, with $\tilde{E}_u$ the unobstructed disturbance at P. Equation (1.12) can be evaluated using the Fresnel integrals, $C(w)$ and $S(w)$:

$$\int_0^w e^{i\pi w'^2/2} dw' = C(w) + iS(w) \tag{1.13}$$

$$S(w) = \int_0^w sin\left(\frac{\pi w'^2}{2}\right) dw' \tag{1.14}$$

$$C(w) = \int_0^w cos\left(\frac{\pi w'^2}{2}\right) dw' \tag{1.15}$$

Using Eq. (1.13), where $C(w)$ and $S(w)$ are the Fresnel integrals as in Eqs. (1.14) and (1.15), Eq. (1.12) can then be transformed into an intensity, by taking the absolute value and squaring, yielding Eq. (1.16):

$$I_p = \frac{I_u}{4}\{[C(u_2) - C(u1)]^2 + [S(u_2) - S(u_1)]^2\} \times \{[C(v_2) - C(v_1)]^2 + [S(v_2) - S(v_1)]^2\} \tag{1.16}$$

Equation (1.16) gives the intensity of the field at the point P on axis for a square aperture where I_u is the unobstructed intensity at the point P.

As the mathematics of calculating the optical disturbances at all points on a plane at point P is difficult, instead the aperture is moved by small displacements, with $\overrightarrow{SOP}$ fixed. This effectively achieves the translation of the origin, O, with respect to the fixed aperture. Thus, for each displacement new aperture coordinates $y_1, y_2, z_1,$ and z_2 are generated and therefore new $u_1, u_2, v_1,$ and v_2. Therefore the intensity at a point $P + \delta d$, where δd is the displacement, can be calculated. This approximation holds for displacements that are small compared to the ρ_0 [4,8,9]. Using this method and Eq. (1.16) gives the theoretical curves curves in Fig. 1.5.

In φMC, the above experiment is simulated. A square slit is uniformly sampled in the y, and z direction in order to get the packets initial position. A random direction is then sampled, ensuring that the direction points towards the detector screen.

The detector screen's distance from the aperture is then varied and the intensity on the screen is measured for $\sim 10^{10}$ photons released from the aperture, as Huygens wavelets. For *Fresnel numbers* greater than 1.0, the number of bins is 300, covering a distance of 600 μm. For the case of Fraunhofer diffraction, the number of bins is 100 covering a distance of 6000 μm. The simulations take ~ 3 minutes for 10^{10} packets to be run on an Intel Xeon E3–1245 v5, 8 cores @ 3.5GHz machine. The number of bins, and photons packets simulated had to be increased for the cases where the Fresnel number was large (i.e the detector screen was near the aperture) Fig. 1.5 shows the comparison between the theory and the φMC simulations.
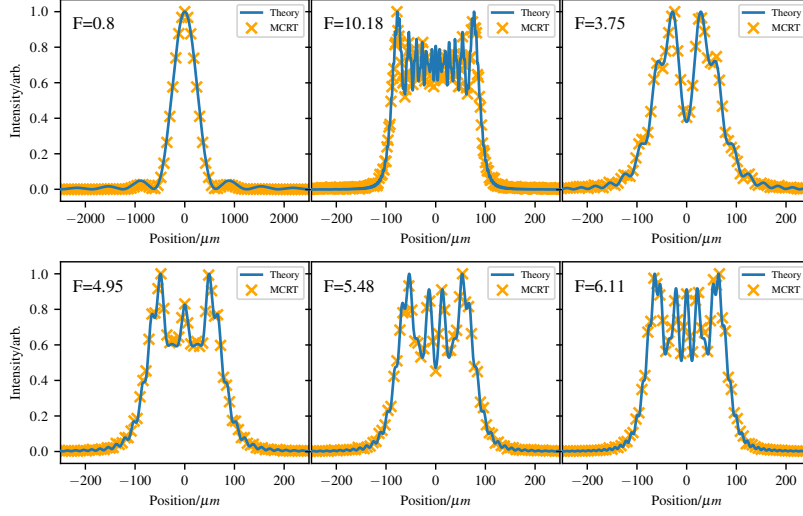
Figure 1.5: *Comparison of theory and simulation for diffraction through a square aperture in the Fresnel and Fraunhofer regimes.*

1.3 Bessel Beams

Bessel beams, as described in the introduction to this chapter, are "non–diffracting" beams, that can "self heal". This means, in reality, that the central core of the beam does not spread out, and that if a blockage is placed in front of the beam, the beam reforms further down the optical axis. There is some debate amongst physicists as to weather these phenomena are justly labelled, or if they glib terms used to make Bessel beams seem like the solution to everything.

The first "complex" beam simulated using φMC is a Bessel beam. Bessel beams are non-diffractive solutions to the wave equation. Bessel beams were first shown to blah
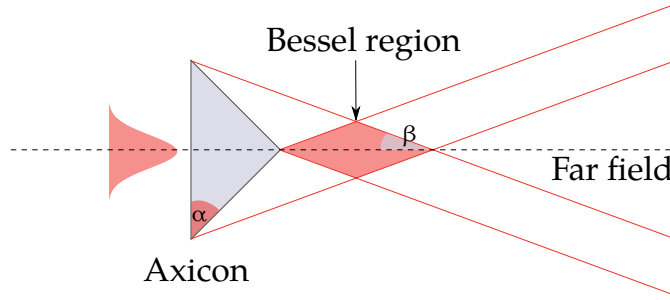

Figure 1.6: *Geometry of a Bessel beam, generated by an axicon lens. β is the angle with the optical axis, and the angle of the conical waves. α is the axicon angle.*

From the scalar description of the electric component of the beam, we get:

$$E(r, z) = E_0 \sqrt{\frac{2\pi k z w_0 sin(\beta)}{z_{max}}} \exp^{\left(-\frac{z^2}{z_{max}^2} - \frac{i\pi}{4}\right)} J_0\left(kr sin(\beta)\right) \exp^{(ikz cos(\beta))} \tag{1.17}$$

Where:

k is the wavevector, $k = \frac{2\pi}{\lambda}$ $[m]$;

z is the distance from the axicon tip $[m]$;

β is the angle the wavefront propagates at (see Fig. 1.6) $[rad]$;

w_0 is the $\frac{1}{e^2}$ width of the input Gaussian beam $[m]$;

J_0 is the Bessel function of the first order;

r is radial distance from the optical axis $[m]$.

Equation (1.17) gives the electric field for a Bessel beam. The intensity can be calculated using:

$$I(r,z) = \frac{c\epsilon_0 \left|E_0\right|^2}{2} \tag{1.18}$$

Using the definition total power transmitted by a beam as:

$$P = \frac{\pi I_0 w_0^2}{2} \tag{1.19}$$

Where I_0 is defined as on axis intensity of the incident Gaussian beam.

$$I_0 = \frac{c\epsilon_0 E_0^2}{2} \tag{1.20}$$

Substituting Eqs. (1.17), (1.19) and (1.20) into Eq. (1.18) yields:

$$I(r,z) = \frac{4k_r P}{w_0} \frac{z}{z_{max}} J_0^2\left(k_r\ r\right) \exp\left(-\frac{2z^2}{z_{max}^2}\right) \tag{1.21}$$

Where:

k_r is the radial wavevector, $k_r = k\sin(\beta)$;

P is the power of the incident Gaussian beam.

To check out method accurately models Bessel beams, we compare out beam to theoretical expressions and experimental data.

To compare against a theoretical Bessel beam, a Bessel beam is modelled in the MCRT phase simulation, and propagated through air past the "Bessel region". A slice of the intensity is then plotted against what the theory predicts the Bessel beam should look like. A check of how the Bessel beam propagates in the far field is also preformed.

Equation (1.21) gives the profile of a theoretical Bessel beam at a depth z_{max}, this is plotted against the simulation when $\frac{4k_r P z}{w_0 z_{max}} e^{-2\left(\frac{z}{z_{max}}\right)^2} = 1$, with the simulation similarly normalised, by normalising to the maximum intensity of the image generated. Figure 1.7 shows this comparison.

To ensure our algorithm works in turbid media, we carried out an experiment where a Bessel beam was propagated through a medium of varying turbidity. A laser, wavelength 488 nm, with a Gaussian profile is shone on an axicon lens, with angle 5 °. The laser beam had a $\frac{1}{e^2}$ spot size of 2 mm. The Bessel beam was allowed to propagate through the air for 10 cm before entering a cuvette of side 2 mm. The cuvette was filled with 500 μL of water, and various volumes of a scattering agent added. The scattering agent used is intralipid 20 % (Sigma-Aldrich), which is diluted as shown in Table 1.1. Dilutions of Intralipid are kept below 2% scattering particle concentration, so that the scattering exhibited by the intralipid is in the independent scattering regime. This allows the linear scaling of the optical properties by concentrations [10–12]. Images of the Bessel beam as it emerges from the cuvette are taken for comparison with out algorithm. Figure 1.8 shows the experimental setup.
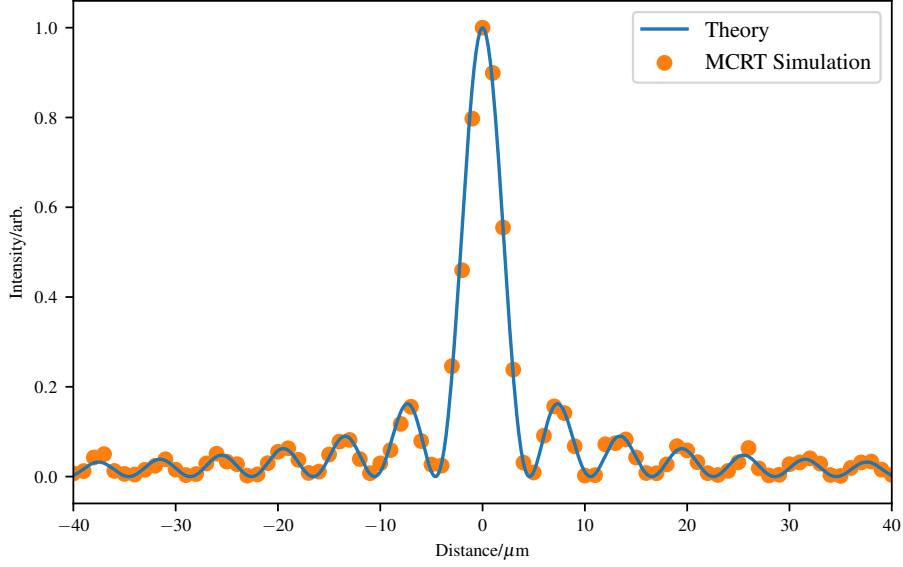
Figure 1.7: *Comparison of theoretical and MCRT simulation of a Bessel beams, with intensity normalised. The results from φMC show good agreement with the theory.*
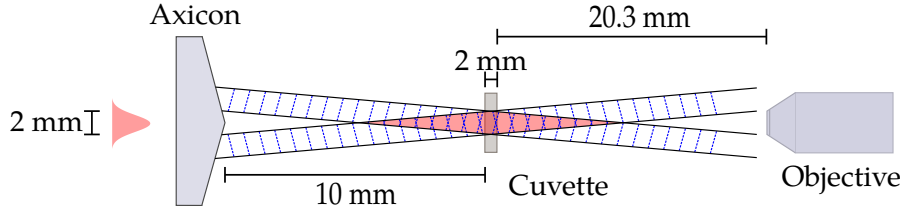

Figure 1.8: *Experimental setup for propagating a Bessel beam through a cuvette filled with varying concentrations of Intralipid 20%. Bessel beam is imaged by an 20× objective lens and a Grasshopper 3 camera.*

Volume/μL		Intralipid concentration	
Intralipid	H_2O	Volume/%	Scattering particle/%
0	500	0.0	0.0
2	500	0.39841	0.0908
4	500	0.79365	0.1816
6	500	1.18577	0.2724
8	500	1.57480	0.3632
10	500	1.96078	0.4534
12	500	2.34375	0.5448

Table 1.1: *Intralipid solutions used for experiment.*

To model within φMC, the experimental setup we simplify the setup considerably. The simulation models the propagation of a photon packet through the axicon to its conical surface. On the conical surface the Huygens-Fresnel principle is invoked, and the packet is sampled onto the surface of the medium (cuvette). The sampling of the photon onto the surface of the medium, speeds the algorithm up, as it does not need to simulate the photons that would "miss" the medium. From there the usual MCRT method propagates the packet through the medium while tracking its phase, and scattering the packet until it leaves the medium. If the packet leaves the medium to any side other than the far side of the cuvette (e.g any side of the cuvette not facing the objective lens), then it is discarded. If the packet leaves the medium on the objective lens facing side, then the packet is recorded by its phase onto an area element. For each intralipid concentration 3.2×10^{11} photons are run over 32 cores, taking ~ 4 hours for the 0.5448% intralipid concentration. Once all the photon packets have been run, the image is the phase is converted into intensity, as in Eq. (1.2), but in 2D.

Figure 1.9 shows the results from the experiment and simulation. The simulation shows good agreement with experimental data.
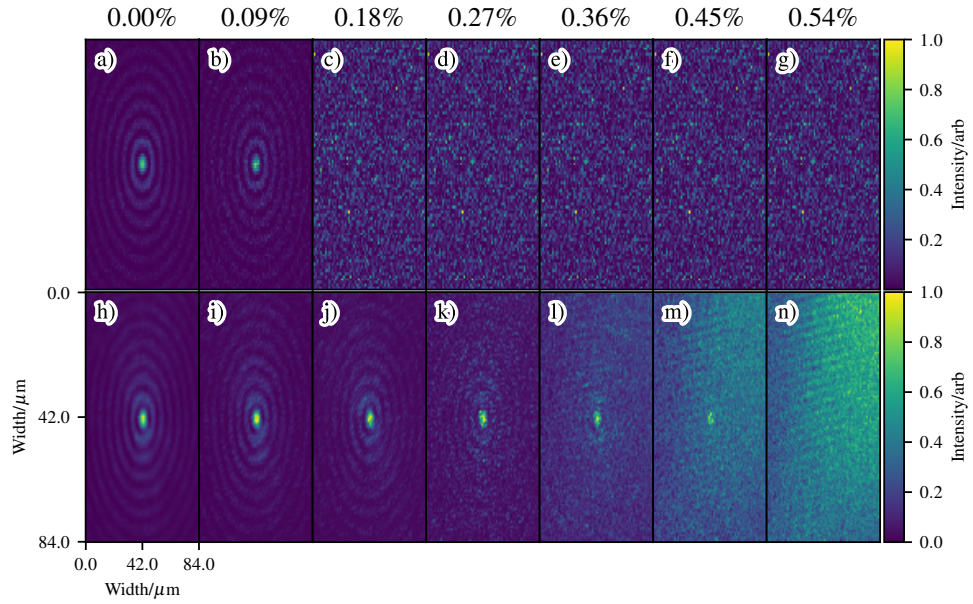

Figure 1.9: *Comparison of experimental and simulation data for propagation of a Bessel beam produced by an axicon, through mediums of various turbidity. Images a) to g) is the data from φMC, and h) to n) are the experimental data. Concentrations along the top are the concentration of scattering particles in each solution as in Table 1.1. All images cropped so they are the same size.*

1.4 Gaussian Beams

1.5 Other Beams

Our technique outlined in the preceding sections, can also be applied to arbitrary non-diffracting or complex beams. The only requirements for our algorithm to be able to model a complex beam, is that there is some phase delay that can be modelled analytically*.

The first example of using our algorithm to model complex beams is to model a Laguerre-Gauss beam. A Laguerre-Gauss beam can be created by introducing a helical phase delay to a plane wave blah blah. ***put theory here + phase and interference patterns for all beams

Another example of our algorithms flexibility is that it can also model Hermite-Gauss beams, higher order Bessel beams and airy beams

1.6 Comparison

1.7 Discussion

a [13]

1.8 Conclusion

---

*It may be possible to model phase delays that are not analytical expressions. Simulating spatial light modulators may also be possible with our algorithm.

Bibliography

[1] JJJM Durnin, JJ Miceli Jr, and JH Eberly. Diffraction-free beams. *Physical review letters*, 58(15):1499, 1987.

[2] J Durnin. Exact solutions for nondiffracting beams. i. the scalar theory. *JOSA A*, 4(4):651–654, 1987.

[3] Christiaan Huygens. *Treatise on light.* tredition, 2012.

[4] E. Hecht. *Optics.* Pearson Education, Incorporated, 2017.

[5] Christiaan Huygens, Thomas Young, Augustin Jean Fresnel, and François Arago. *The wave theory of light: memoirs of Huygens, Young and Fresnel*, volume 15. American Book Company, 1900.

[6] Auguste Fresnel. Mémoire sur la diffraction de la lumière. *da p. 339 a p. 475: 1 tav. ft; AQ 210*, page 339, 1819.

[7] G Kirchhoff. Ann. d. physik. *(2)*, 18:663, 1883.

[8] M. Born, E. Wolf, and A.B. Bhatia. *Principles of Optics: Electromagnetic Theory of Propagation, Interference and Diffraction of Light.* Cambridge University Press, 2000.

[9] J.W. Goodman. *Introduction to Fourier Optics.* W. H. Freeman, 2017.

[10] Ben Aernouts, Eduardo Zamora-Rojas, Robbe Van Beers, Rodrigo Watté, Ling Wang, Mizuki Tsuta, Jeroen Lammertyn, and Wouter Saeys. Supercontinuum laser based optical characterization of intralipid® phantoms in the 500-2250 nm range. *Optics express*, 21(26):32450–32467, 2013.

[11] Martha Z Vardaki, Benjamin Gardner, Nicholas Stone, and Pavel Matousek. Studying the distribution of deep raman spectroscopy signals using liquid tissue phantoms with varying optical properties. *Analyst*, 140(15):5112–5119, 2015.

[12] Paola Di Ninni, Fabrizio Martelli, and Giovanni Zaccanti. Effect of dependent scattering on the optical properties of intralipid tissue phantoms. *Biomedical optics express*, 2(8):2265–2278, 2011.

[13] Charles Mignon, Aura Higuera Rodriguez, Jonathan A Palero, Babu Varghese, and Martin Jurna. Fractional laser photothermolysis using bessel beams. *Biomedical optics express*, 7(12):4974–4981, 2016.